HUDSON LABORATORIES of Columbia University

145 Palisade Street, Dobbs Ferry, N. Y. 10522

AD670548

TECHNICAL REPORT No. 138

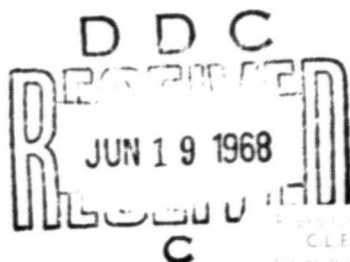# ESTIMATION OF THE STATISTICAL PROPERTIES OF THE OCEAN BOTTOM

Part I: A Survey of Theory and Experiment

Part II: Interpretation of Marine Geophysical Data

by
C. S. Clay

December 1967

D D C

JUN 1 9 1968

C

CLEARINGHOUSE

Hudson Laboratories
of
Columbia University
Dobbs Ferry, New York 10522

Technical Report No. 138

ESTIMATION OF THE STATISTICAL
PROPERTIES OF THE OCEAN BOTTOM

Part I: A Survey of Theory and Experiment
Part II: Interpretation of Marine Geophysical Data

by

C. S. Clay

UNCLASSIFIED

December 1967

This report consists   Copy No. ?℃
of 67 pages   of 145 copies

ABSTRACT

The reflection and scattering of acoustic signals by the bottom of the ocean depend upon the physical properties of the bottom and the wavelength spectrum of the signals. On the basis of the frequency and grazing angle dependence of the reflected or scattered signals, physical properties such as the densities, acoustic velocities of subbottom layers, and the rms roughness of the layers can be estimated.

TABLE OF CONTENTS

PREFACE

This report has been written in two parts. Each of the parts is quite independent and yet each part covers much of the same material. Their difference lies in that Part I is a development of the subject, whereas in Part II certain simplified results are applied directly to marine geophysical problems.

While Part II was written first and was intended to assist in the interpretation of the marine geophysical surveys, the existence of Part I as a reference was assumed. Part I formed the basis of an invited paper presented at the 74th Meeting of the Acoustical Society of America, Miami Beach, Florida, November 1967.[*]

C. S. Clay[†]

---

[*] C. S. Clay, "Measurement of the ocean bottom," J. Acoust. Soc. Am. <u>42</u>, 1183 (A) (1967). (HL Inf. Doc. No. 139.)

[†] Dr. Clay is now Professor of Geophysics, Department of Geology and Geophysics, University of Wisconsin, Madison, Wisconsin.

PART I. THEORY AND EXPERIMENT

1. Interaction of Sound at the Bottom – Interpretation

Our purpose is to examine rather carefully the interpretation of measurements of the interaction of acoustic signals with the bottom of the ocean. We have avoided the words "reflected, " "scattered, " or "diffracted" because these words describe a particular mechanism and method of data analysis.

The basic measurement is made as shown in Fig. 1. The source transmits a transient signal so that the sound that interacts with the bottom can be separated from other paths such as the direct path or multiple surface and bottom paths. The bottom has been drawn as being a black box, and we don't know much about it except that it is passive. It is also bounded in the sense that we can confine the sound field to a given region of the bottom.
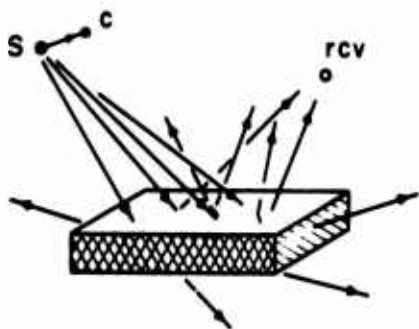
Fig. 1. Interaction of sound with the ocean bottom. S is the source, C is the calibration receiver, and rcv is the receiver. The ocean bottom is inside an imaginary black box.

We now have a measurement of the acoustical signal at the receiver. The positions of the source, receiver, and insonified region are known. Signal processing equipment for filtering, correlating, squaring, displaying, etc. is available and so we need not discuss that. The question is how can we use the geometry of the measurement to measure the interaction at the bottom. We stress the word "how" because the way we chose to work up the data requires an assumption about the nature of the interaction.

The procedure we follow is trial and error. That is, we assume a description of the bottom and then calculate theoretical received signals (with or without signal processing) for a number of different geometries. Depending upon how good the comparison of the theoretical and experimental measurements is, we use the description or try again.

2. Reflecting Bottom

Let us assume the box to be a reflector for the first trial. The consequence of this assumption is shown in Fig. 2. By means of the geometry and calibration, we compute the ratio of the measured signal P_{meas} to the theoretical signal $P_{th, r}$ for a unit perfect reflector. The ratio is termed the apparent reflection coefficient $\mathbb{R}_a$.[*] We use the word "apparent" because $\mathbb{R}_a$ is the result of an interpretation or assumption, and not a direct measurement.

---

[*] In text and equations $\mathbb{R}$ substitutes for script R .
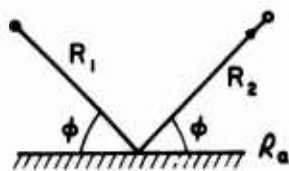
$$p_{th,r} = \frac{p_0}{R_1 + R_2}$$

$$R_a = \frac{p_{meas}}{p_{th,r}}$$

$$(p_{th,s})^2 = \frac{p_0^2 A}{R_1^2 R_2^2}, \quad S = 1$$

$$S_a = \frac{(p_{meas})^2}{(p_{th,s})^2}$$

Fig. 2. Reflection at the bottom; p_0 is the signal at unit distance.

Fig. 3. Scattering at the bottom; A is the illuminated area and its dimensions are much less than R_1 and R_2 .

3. Scattering Bottom

We could have assumed the bottom to be so rough that it scatters energy into all directions. The scattering interpretation is shown in Fig. 3. For illustration, the density-velocity contrast at the bottom is assumed to be so large that each small facet of the bottom can be regarded as being a perfect reflector. The apparent scattering coefficient is S_a . As in the previous example, S_a is the result of an interpretation. Comparison of the dependence of $p_{th,\,r}$ and $p_{th,\,s}$ upon the geometry shows that R_a is a function of $\left(R_1 + R_2\right)^{-1}$ whereas S_a is a function of $\left(A R_1^{-2} R_2^{-2}\right)$.

These two very different interpretations can be applied to the <u>same</u> <u>measurement.</u> It is obvious that we need to know whether the bottom is smooth or rough so as to know how to work up our data. Let us look at

a geological and geophysical conception of the bottom of the ocean – as shown in Fig. 4. This somewhat artistic drawing is based upon a great deal of knowledge. Most of it was obtained by means of echo sounders, bottom samples, deep sea cameras, and seismic profilers. Generally, it is a good picture, but we probably should not use it to describe the bottom precisely enough to predict the result of a particular measurement. The reason is that our measurements are sensitive to details that are not ordinarily shown or measured. These charts can be used as a guide for our first guess, but in the end the measurements must be used to make a description of the bottom.
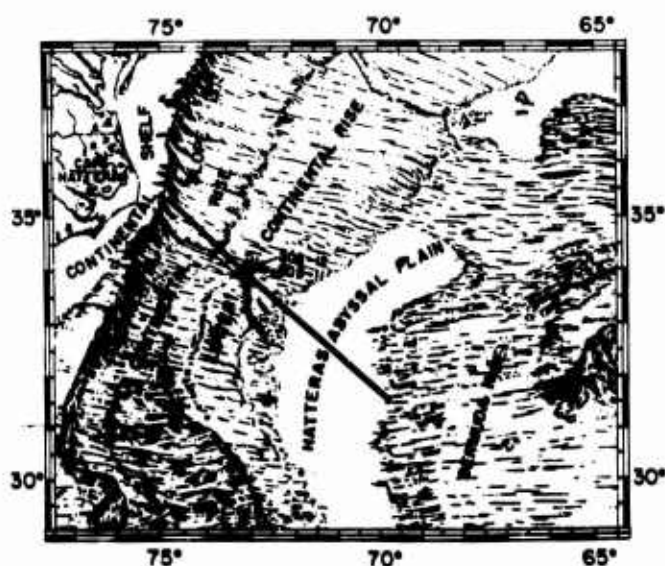

Fig. 4. Heezen and Tharp[1] pictographic chart of the ocean bottom.

4. Reflection and Scattering of Sound by an Irregular Interface – Theory

The theory of scattering of waves by an irregular surface has been the subject of a number of papers and is treated in several books. The first formulation was given by Rayleigh. Brekhovskikh[2] and Eckart[3]

-5-

have given solutions based on the Helmholtz equation. Eckart's formulation is particularly convenient for the study of reflection and scattering by a randomly rough surface.

The development given by Tolstoy and Clay[4] is essentially that of Eckart, and it is convenient to follow their notation. We make the simplifying assumption that the source and receiver are very far away from the illuminated area. On neglecting the slopes of the surface, their Eq. (6.19) is

$$p = \frac{-iBe^{ik(R_1+R_2)}}{2\pi R_1 R_2} \int D \, \mathbb{R} \gamma \, e^{2i(\alpha x+\beta y+\gamma \zeta)} \, dy \, dx \tag{1}$$

$$2\alpha = k\left(\sin \theta_1 - \sin \theta_2 \cos \theta_3\right)$$

$$2\beta = -k\left(\sin \theta_2 \sin \theta_3\right)$$

$$2\gamma = -k\left(\cos \theta_1 + \cos \theta_2\right)$$

$$\kappa^2 = \alpha^2 + \beta^2$$

$$k = 2\pi/\lambda = \omega/c$$

$$B^2 = \Omega \rho c(2\pi)^{-1}$$

D = illumination function

Ω = source power

R_1 is in the x-z plane

θ_3 is the angle between the x-z plane and plane containing R_2 and the z axis

ζ is the elevation relative to z=0

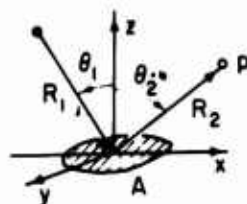$\mathbb{R}$ is the reflection coefficient .

Fig. 5. Geometry for Helmholtz formulation.

$$p \sim \frac{\gamma R}{2\pi R_1 R_2} \int_A D e^{2i(\alpha x + \beta y + \gamma \zeta)} \, d\alpha$$

The geometrical quantities are defined in Fig. 5. We notice that 2α, 2β, 2γ are the differences of the wave numbers along R_1 and R_2. In our approximation, they are constant for particular source and receiver positions. In the specular direction, the horizontal components (α, β) are zero and this considerably simplifies the integral:

$$P\bigg|_{\substack{\alpha=0 \\ \beta=0}} \simeq \frac{-i\gamma \, \mathbb{R} \, e^{ik(R_1+R_2)}}{2\pi R_1 R_2} \int D \, e^{2i\gamma\zeta} \, dy \, dx \quad . \qquad (2)$$

The mean square acoustic pressure is

$$\langle PP^* \rangle = \frac{\gamma^2 \, \mathbb{R}^2 B^2}{4\pi^2 R_1^2 R_2^2} \int \int \int \int D \, D'' \, \left\langle e^{2i\gamma(\zeta - \zeta'')} \right\rangle \, dy \, dx \, dy'' \, dx'' \quad . \qquad (3)$$

The average is taken over the random surface. We assume the distributions of ζ and ζ'' to be Gaussian and that difference $(\zeta' - \zeta'')$ depends upon their separation. Thus, the substitution of the bivariate Gaussian function and the evaluation of the average yield the following:

-7-

with
$$W = \frac{1}{2\pi\sigma^2(1-\psi^2)} \quad \exp - \left\{\frac{\zeta^2 + \zeta''^2 - 2\zeta\zeta''\psi}{2\sigma^2(1-\psi^2)}\right\} \tag{4}$$

$$\psi = \frac{1}{\sigma^2}\langle \zeta\zeta''\rangle \tag{5}$$

$$\sigma = \text{rms roughness.}$$

$$\langle pp^*\rangle = \frac{\gamma^2 \mathbb{R}^2 B^2}{4\pi^2 R_1^2 R_2^2} \int\int\int\int D\,D''\, e^{-4\gamma^2\sigma^2(1-\psi)}\, dy\,dx\,dy''\,dx'' \quad . \tag{6}$$

We have chosen to use a Gaussian type of illumination function because it resembles the main lobes of array responses and has no side lobes. With the aid of the assumption that x depends only upon $(x-x'')$ and $(y-y'')$, the following substitutions permit the integration of (6)

$$D = e^{-(x^2/2X^2)-(y^2/2Y^2)} \quad , \quad D = e^{-r^2/R^2} \tag{6a}$$

$$x'' = x-\xi$$

$$y'' = y-\eta$$

$$\langle pp^*\rangle = \frac{\gamma^2 \mathbb{R}^2 B^2 XY}{4\pi R_1^2 R_2^2} \int\int \exp -\left\{\frac{\xi^2}{4X^2} + \frac{\eta^2}{4Y^2} + 4\sigma^2\gamma^2(1-\psi)\right\} d\xi\,d\eta \tag{7}$$

or

$$\langle pp^*\rangle = \frac{\gamma^2 \mathbb{R}^2 B R^2}{2R_1^2 R_2^2} \int_0^\infty \exp -\left\{\frac{r^2}{2R^2} + 4\gamma^2\sigma^2(1-\psi)\right\} r\,dr \quad . \tag{8}$$

For general forms of ψ , Eqs. 7 and 8 are rather difficult to integrate and it has been customary to examine the high- and low-frequency cases separately:

$$\text{high frequency} \quad 4\gamma^2\sigma^2 \gg 1$$
$$\text{low frequency} \quad 4\gamma^2\sigma^2 \ll 1 \quad .$$

Perhaps we can illustrate the difference between the high and low cases, or the smooth and rough bottoms by referring to Fig. 6. The upper profile was taken over an area presumed to be rough. The dissimilarity of the reflected signal from one ping to the next is quite evident. Although we can follow reflection interfaces, the reflection signals appear somewhat sporadically. The lower profile was taken over a smooth area and here the signals from the reflection interfaces are much easier to follow.
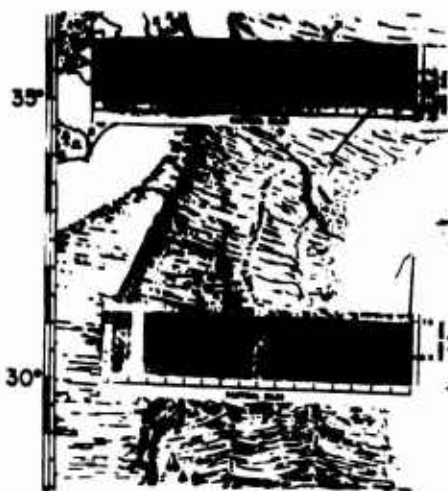

Fig. 6. Continuous seismic profiles taken over smooth and rough bottoms.

The reader may have noticed that we have said very little about the reflection coefficient. We assume $\mathbb{R}$ is the reflection at the water bottom interface and can include subbottom layers. It is given in the appendix and is discussed in more detail by Tolstoy and Clay (Ref. 4, Sections 2.4 and 2.5).

5. The Illumination and Bottom Roughness

The roughness of the bottom can be exceedingly complex. σ^2 and ψ are unknown and are the quantities that we are hoping to determine. As we mentioned earlier, our procedure is to make a guess, test it, and then improve our guess. A few remarks about the form of ψ for several expected types of bottom should be helpful. In this it is important to recognize that the illumination function limits our field to the illuminated area and that we are considering only the roughness over the illuminated area. As shown in Fig. 7, roughness outside the illuminated area does not matter — at least so long as it does not cause shadows. A bottom that appears to be moderately rough on an echo sounding profile could be smooth over the illuminated area as sketched in Fig. 8. These examples show that we are concerned about bottom irregularities that have wavelengths less than the dimensions of the illuminated area, X and Y .

Correlation functions, ψ , are sketched in Fig. 9 for typical bottom types. The correlation function can be regarded as being zero for distances greater than L . We shall use these properties in our approximate evaluations of the integral.
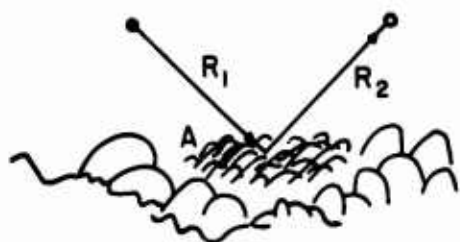
Fig. 7. The illuminated area.
The area is indicated by the
shading on the bottom profile.
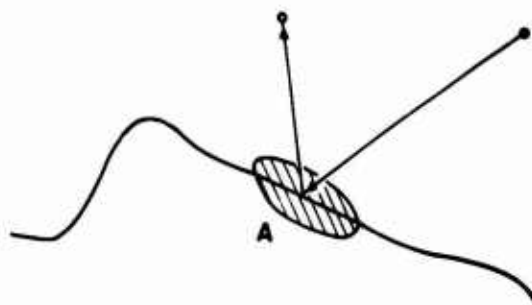
Fig. 8. Smooth bottom over A ,
the illuminated area.
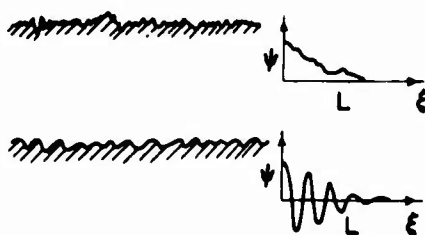
Fig. 9. Bottom profile and correlation functions

6. High-Frequency Signals, $(\gamma\sigma)^2$

Much of the ocean has a bottom that can be considered rough for

most of the frequency range used in geophysical and sonar applications.

Generally speaking, the bottom is rough when the rms roughness is

many acoustical wavelengths.

A number of experiments have shown that the sound is scattered

incoherently and we can then recast the form of the equation for $\langle pp^* \rangle$.

It is convenient to rewrite Eq. (8) so that the integral is proportional to a scattering function. In doing this, we are assuming the validity of the incoherent scattering interpretation. With the aid of Eq. (8), let us define the high-frequency scattering function and other quantities as follows:

$$S = \frac{\gamma^2 R^2}{2\pi} \int_0^\infty D \exp[-4\gamma^2\sigma^2(1-\psi)] \, r dr \qquad \text{for} \qquad \gamma^2\sigma^2 \gg 1 \qquad (9)$$

$$\langle pp^* \rangle = p_1^2 A S / R_2^2 \qquad (10)$$

$$p_1^2 = B^2 / R_1^2 \qquad (11)$$

$$A = \pi R^2 \qquad (\text{or } XY) \quad . \qquad (12)$$

Our purpose in introducing S is to separate the scattering function so that we can display more easily its dependence upon frequency, angle, and ψ . On referring to Fig. 3, S can also be written as

$$S = \langle pp^* \rangle / \left(P_{th, \, s} \right)^2$$

$$\left(P_{th, \, s} \right)^2 = p_1^2 A / R_2^2 \quad .$$

Eckart[3] suggested that the integral in (9) can be evaluated rather easily by recognizing that the principal contribution comes from the very small values of r and that the integral is nearly zero for r greater than the correlation distance L . Also, the illumination function D assures us of convergence for large r . It has been customary to

assume an exponential form for ψ and then to expand ψ as a power series.[3,5] Depending upon which terms are kept, one finds the scattering function to have quite different dependencies upon frequency. For illustration, we calculate S for the following simple types of ψ.

$$\psi = a \qquad\qquad 0 \leq r \leq L$$
$$\psi = 0 \qquad\qquad r > L \qquad\qquad\qquad (13)$$
$$a \leq 1$$

$$\psi_q \sim e^{-r^2/2L^2} \qquad,\text{ or }\quad \psi_q = 1-r^2/2L^2 \qquad 0 \leq r \leq 2L^2$$
$$\psi_q = 0 \qquad\qquad r^2 > 2L^2 \qquad\qquad (14)$$

$$\psi_\ell \sim e^{-r/L} \qquad,\text{ or }\quad \psi_\ell = 1-r/L \qquad 0 \leq r \leq L$$
$$\psi_\ell = 0 \qquad\qquad r > L \qquad . \qquad\qquad (15)$$

These functions are illustrated in Fig. 10. The double cross hatch indicates the region that makes the main contribution to the integral. The skirts of the correlation function are probably unimportant.
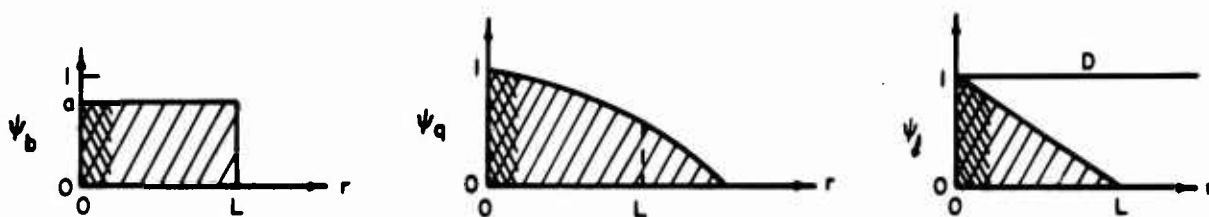

Fig. 10. ψ for high-frequency approximation.

-13-

The dependence of D upon r has also been sketched on ψ_{ℓ} to show that D is nearly one over the range of values of R for which ψ is different from zero. We can make an approximate evaluation of (9) by assuming that D is one over the range of r from zero to L. The value of the integral over D for $X = 0$ gives an estimate of the magnitude of the errors involved in the approximations as follows:

$$S\Big|_{\psi=0} = \frac{\gamma^2 \mathbb{R}^2}{2\pi} \int_0^\infty D\, e^{-4\gamma^2 \sigma^2}\, r\, dr \qquad (16)$$

$$= \frac{\gamma^2 \mathbb{R}^2}{4\pi} R^2 e^{-4\gamma^2 \sigma^2} \qquad . \qquad (17)$$

For $\gamma^2 \sigma^2 = 10$, the exponent in Eq. 17 is of the order of e^{-40}. The other factors in (17) are probably less than 10^7 (or e^{16}) for $R \simeq 1000\, \lambda$, and (17) is less than e^{-24} or about -100 dB. The scattering functions are the following:

$$\psi_b \quad , \quad S_b \simeq \frac{\mathbb{R}^2}{4\pi} \gamma^2 L^2 \exp\, -[4\gamma^2 \sigma^2 (1-a)] \qquad (18)$$

$$\psi_q \quad , \quad S_q \simeq \frac{\mathbb{R}^2}{8\pi} \frac{L^2}{\sigma^2} \qquad (19)$$

$$\psi_{\ell} \quad , \quad S_{\ell} \simeq \frac{\mathbb{R}^2}{32\pi \gamma^2 \sigma^2} \left(\frac{L^2}{\sigma^2}\right) \qquad . \qquad (20)$$

The dependence of these three functions upon grazing angle is shown in Fig. 11. For illustration, the following parameters were chosen:

$$\gamma^2 \sigma^2 = 10 \qquad \psi_b = 0.9 \qquad 0 \le r \le L$$

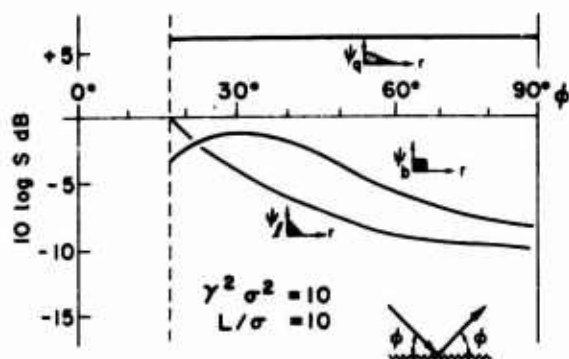$$L/\sigma = 10 \qquad \gamma L = 10 \qquad .$$

Fig. 11. Comparison of the high-frequency scattering functions in specular direction as a function of grazing angle. ($\gamma^2\sigma^2 = 10$, $L/\sigma = 10$, $\psi_b = 0.9$.)

The scattering function in the specular direction is independent of angle and frequency for quadratic type approximations to ψ , Eqs. (14) and (19). Other approximations, such as the box and linear functions, show angle and frequency dependence. The type of correlation function also changes the magnitude of the scattering function, even though the values of σ and L are the same.

The scattering of sound into directions other than the specular also depends upon the type of correlation function. For non-specular scattering, we calculate the mean square of Eq. (1) and reduce the multiple integrals. After some manipulation, one obtains the following for the isotropic case:

$$S \simeq \frac{\gamma^2 \mathbb{R}^2}{2\pi} \int_0^\infty J_o (2\kappa r) \exp\left[-4\gamma^2\sigma^2(1-\psi)\right] r\,dr \qquad (21)$$

where D has been replaced by 1 in view of the rapid convergence of the integrand. The scattering functions for ψ_q and ψ_ℓ are:

-15-

$$S_q \simeq \frac{R^2}{8\pi} \left(\frac{L^2}{\sigma^2} \right) \exp - \frac{L^2 \kappa^2}{2\gamma^2 \sigma^2} \tag{22}$$

$$S_\ell \simeq \frac{R^2}{4\pi} \frac{\gamma^2 L^2 \gamma^2 \sigma^2}{(4\gamma^4 \sigma^4 + \kappa^2 L^2)^{3/2}} \qquad . \tag{23}$$

For the general case, γ and κ are functions of the directions to the source and receiver as shown in Fig. 5. High-frequency scattered sound has been studied extensively by C. W. Horton and others at the University of Texas. The comparison of theory and experiment shown in Fig. 12 was taken from Horton et al.[6] In a preceding paper, Horton and Muir[5] show that some modification of the surface boundary condition is needed to improve the theoretical fit to the data. Their modification appears to be approximately a shadowing factor. Their expression for S_ℓ is (in our notation)

$$S_\ell = \frac{R^2}{16\pi} \frac{\gamma^2 L^2 \gamma_2^2 \sigma^2}{(4\gamma^4 \sigma^4 + \kappa^2 L^2)^{3/2}} \tag{23a}$$

$$\gamma_2 = k \cos \theta_2 \qquad .$$

The correlation function of their rough surface had an approximately linear form for small r . The example we have chosen is for vertically incident sound.
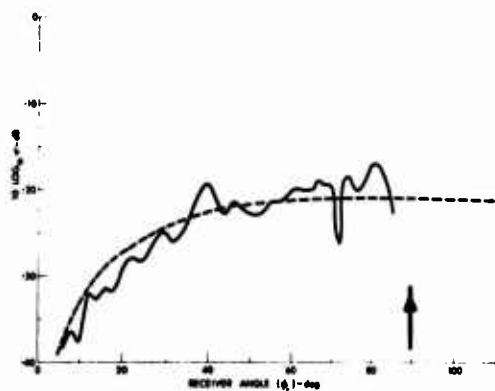
Fig. 12. The scattering coefficient for the high-frequency case.[6] The dashed line is Eq. 24a. f=100 kHz, σ =0.92 cm , L=6.5 cm , $k\sigma$ =3.9 . The receiver angle is grazing angle and the arrow indicates the source position, 90° grazing angle.

For a second illustration, we use the so-called reverberation and determine the back-scattering functions, i.e., $\theta_2 = -\theta_1$. The back-scattering functions for ψ_q and ψ_ℓ are shown in Fig. 13. The strong scattering of sound in the specular direction ($\phi = 90°$ grazing angle) is quite evident for the bottom having the quadratic correlation coefficient. A bottom having a linear correlation coefficient scatters sound much more diffusely.
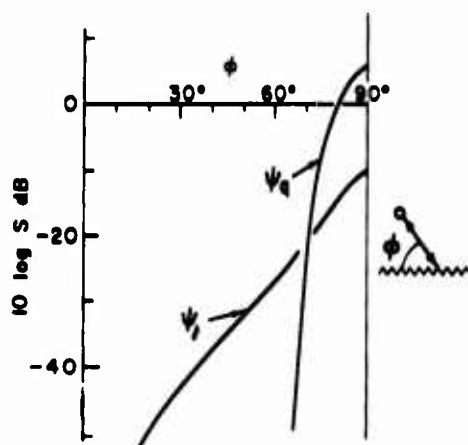

Fig. 13. Back-scattering functions. ($\gamma^2\sigma^2 = 10$, $L/\sigma = 10$.)

-17-

The bottom scanning sonar "looks" at the back scatter and changes
of bottom type may show as high or low scattering areas. The lateral
echo sounder version is shown in Fig. 14. The transducer transmits a
short ping and the travel time, T , of the returning sound depends
upon range and angle. The intensity of the signal is given by Eq. (10)
and is approximately the following:

$$\langle p^2 \rangle \ \sim \ T^{-4} A S$$

where $\qquad\qquad A \ \sim \ T \Delta T \ \text{(angular beam width)} \qquad .$

Since $\langle p^2 \rangle$ decreases as T^{-3} , it is evident that the receiver must
have a very wide range of time-varying gain and/or automatic gain control.
The instruments are usually operated about one-fifth their maximum range
above the bottom and the variation of $\langle p^2 \rangle$ would be expected to be
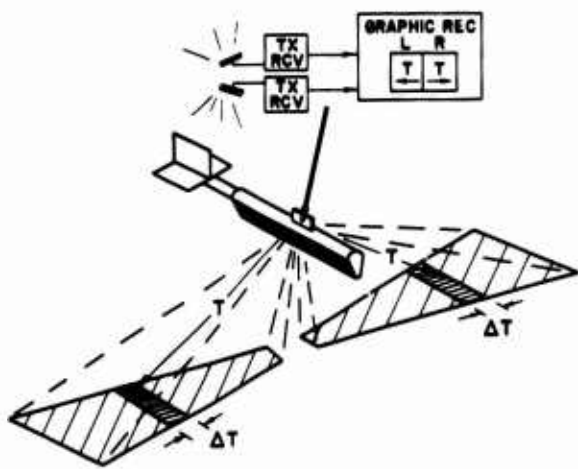larger than 10^4.

Fig. 14. Lateral echo sounder.

Two examples of lateral echo sounder records are shown in Fig. 15. The featureless record was taken in a smooth area and the other was taken in a rougher area. The rough area shows changes of back scatter that are probably due to changes of slope. Light areas or shadows are usually to the left.
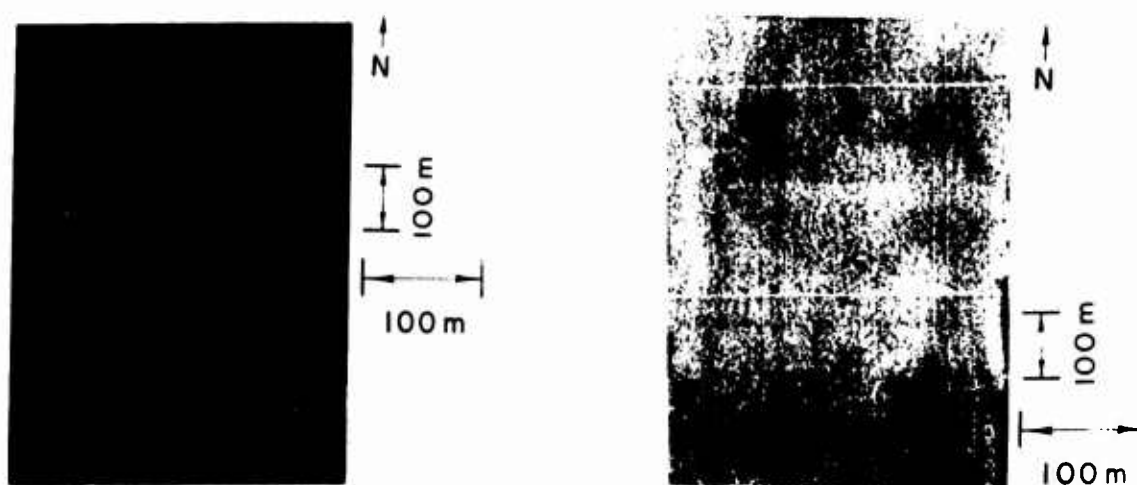
Fig. 15. Lateral echo sounder records. [7]
(Darker is stronger back scatter.)

In summary, the dependence of the high-frequency scattering coefficient upon frequency and angle can be used to guess L/σ and the dependence of ψ upon r for small r .

7. Low-Frequency Signals, $\gamma\sigma < 1$

Studies of acoustical experiments performed over relatively smooth bottoms have shown that the energy is largely reflected and that only a small fraction is scattered. Since the Helmholtz equation yields a solution

that is superficially similar to the incoherent scattering solution, we think it desirable to commence our discussion of the reflection interpretation by considering Eq. (1).

We follow a line of reasoning suggested by Eckart and discussed in detail by Tolstoy and Clay.[4] Let us assume that an acoustic interaction experiment such as shown in Fig. 1 is repeated many times. But in between each repetition, the black box is changed so that each received signal is different. If the properties of the black box are assumed to have a statistical distribution, then one can average over the distribution function.

Let us assume that ζ , the roughness, has a Gaussian distribution over the illuminated area. The average of p over a surface having an rms roughness σ is

$$\langle p \rangle \;=\; \frac{-iB\gamma e^{\,ik(R_1+R_2)}}{2\pi R_1 R_2} \; e^{-2\gamma^2\sigma^2} \; \mathbb{R} \int \int D \, e^{2i(\alpha x + \beta y)} dy \; dx \quad .(24)$$

Notice that for $\sigma = 0$, or a perfectly smooth surface, the form of (24) remains the same. Equation (1) or (24) for $\zeta = 0$ or $\sigma = 0$ is the Helmholtz way of expressing the signal reflected when the surface is illuminated by means of a directional source (6a).

$$p\,\Big|_{\sigma=0} \;=\; \frac{-i\gamma BXY}{R_1 R_2} \; \mathbb{R} \; \exp\left\{-2\alpha^2 X^2 - 2\beta^2 Y^2 + ik(R_1 + R_2)\right\} \quad . \tag{24a}$$

Following the idea shown in Fig. 2, it is convenient to define the reflection signal reflected by a perfect reflector as

$$P_{th, r} = \langle p \rangle \Big|_{\sigma=0, \, \mathbb{R}=1} \tag{25}$$

and then express (25) as follows:

$$\langle p \rangle = P_{th, r} \langle \mathbb{R} \rangle \tag{26}$$

$$\langle \mathbb{R} \rangle = \mathbb{R} \, e^{-2\gamma^2 \sigma^2} \quad . \tag{27}$$

The coherent reflection coefficient describes the reflection in the specular direction. Since the signal from an omnidirectional source can be expanded in terms of outgoing plane waves, it is evident that the coherent reflection coefficient can be applied to the omnidirectional source. We can follow this line of reasoning and assert that $P_{th, r}$ can be calculated by the usual image method as shown in Fig. 2.

The coherent reflection coefficient is independent of the surface correlation function. The mean square signal consists of two terms, the reflected sound and the scattered sound. The latter is dependent upon the surface correlation coefficient and, as we shall show for a simple case, measurements of scattered sound can be used to determine the spatial spectrum of the surface.

For low frequencies and small $\gamma \sigma$, the dependence upon $\gamma \sigma$ and ψ can be approximated as follows:

$$\exp -[4\gamma^2\sigma^2(1-\psi)] \simeq (1+4\gamma^2\sigma^2\psi) \, e^{-4\gamma^2\sigma^2} \quad . \tag{28}$$

We substitute (28) into (7) and (8) and find that the first term, or the multiple integral, is independent of ψ and is the square of the mean signal, (24) or (26). The second term involving ψ is the scattered sound. On making these substitutions and recalling (10) – (12), we obtain

$$\langle pp^* \rangle \simeq \langle p \rangle^2 + \frac{\gamma^2 \sigma^2 \mathbb{R}^2}{\pi R_2^2} p_1^2 A \int \int D'' \psi(\xi, \eta) e^{2i(\alpha\xi + \beta\eta)} d\xi d\eta \quad .(29)$$

If ψ vanishes at values of ξ, η much smaller than X and Y , then again the influence of D on the integral can be ignored. The integral is then the two-dimensional Fourier transform of the space correlation function.[5] It can be written as follows:

$$\Psi = \int_{-\infty}^{\infty} \psi(\xi, \eta) e^{2i(\alpha\xi + \beta\eta)} d\xi d\eta \tag{30}$$

where Ψ is the power spectrum of the surface roughness. The substitution of (30) into (29) yields

$$\langle pp^* \rangle \simeq \langle p \rangle^2 + \gamma^2 \sigma^2 \frac{\mathbb{R}^2 A}{\pi R_2^2} \psi \quad . \tag{31}$$

The second term represents the incoherent scattered sound and has the same geometrical dependencies as given in Fig. 3. Equation (31) is also the acoustical analogue of the familiar optical problem of the diffraction grating. Here we use a known continuous wave signal to determine the spectrum of the rough surface rather than a known grating to analyze the spectrum of an unknown signal. ψ and the corresponding Ψ for several simple functions are the following:

-22-

$$\psi_1 = e^{-(\xi^2+\eta^2)/2L^2} \qquad \Psi_1 = 2\pi L^2 e^{-2(\alpha^2+\beta^2)L^2}$$

$$\psi_2 = e^{-(\xi^2+\eta^2)/2L^2}\cos a\xi \qquad \Psi_2 = \pi L^2\{e^{-(a\pm 2a)^2 L^2/2}\}$$

$$\psi_3 = e^{-\frac{|\xi|}{L}-\eta^2/2L^2} \qquad \Psi_3 = \frac{2\sqrt{2\pi}\, L^2 e^{-2\beta^2 L_2^2}}{1+4a^2 L^2}$$

for $L \ll X$ or Y

The correlation functions and corresponding spectrum functions are sketched in Fig. 16. Numerical examples of the total and scattered sound field as a function of a are shown in Fig. 17. The width of the reflected sound field is dependent upon the dimensions of the illuminated area. That is, the larger the illuminated area, the narrower the reflected sound beam. The width of the scattered sound field varies similarly with the correlation distance.
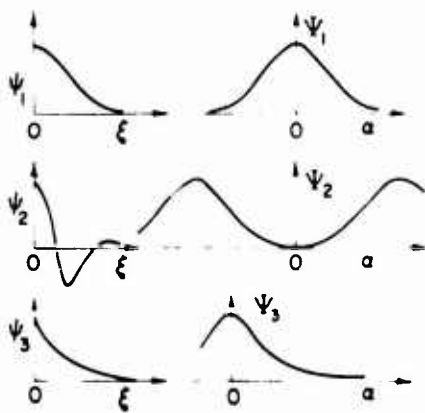

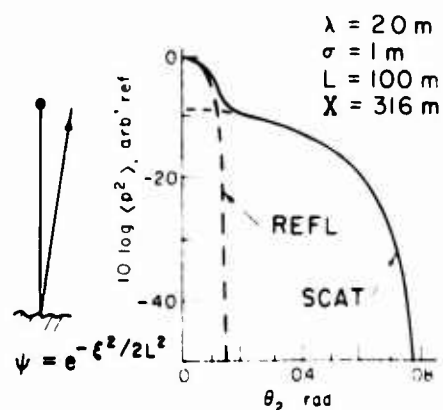Fig. 16. Correlation functions and power spectrum functions.

Fig. 17. Scattered and reflected sound. The surface spectrum is Ψ_1.

In Fig. 18 we show the scattered sound for a peaked spectrum function Ψ_2 as sketched in Fig. 16. The specular reflection is very much narrower than the scattered sound because X^2 is 10 L^2. The width of the scattered sound peaks would be about the same size as the reflected sound for $L^2 \simeq X^2$.
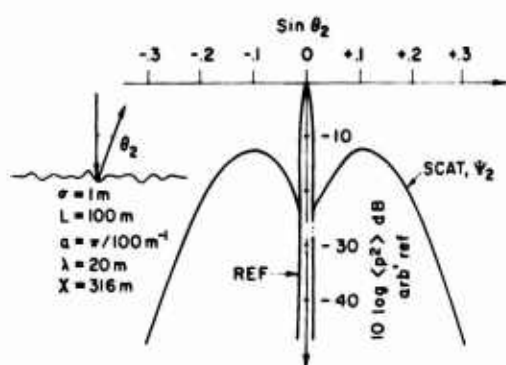

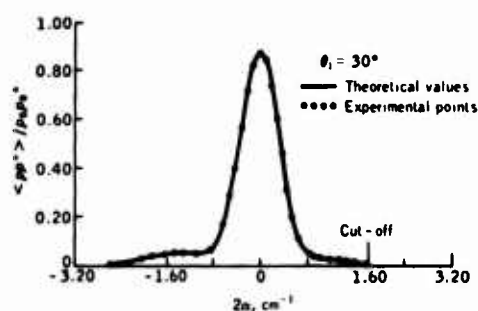Fig. 18. Reflected and scattered sound for Ψ_2.

Fig. 19. Theoretical and experimental scattering of sound for small $\gamma^2 \sigma^2$.[8]

The sound scattered by a surface having a spectrum of the type Ψ_2 was studied by means of laboratory experiments at Brown University. The theoretical curve and data of Proud, Beyer, and Tamarkin[8] are shown in Fig. 19.

We should say a few words about experiments to measure Ψ. First, the scattered sound is proportional to $(\gamma^2 \sigma^2)$ and that was assumed to be small. Thus, the ratio of the scattered sound to the coherently reflected sound is going to be very small. If we were to use an omnidirectional source, then whatever the direction in which we make our

-24-

observation, we will predominantly receive the coherently reflected component. If we confine our experiments to single source and single receiver experiments, then the best that we can do is to measure σ . Perhaps we can separate the coherent component from the scattered component by the use of receiving arrays and thus measure Ψ .

PART II. INTERPRETATION OF MARINE GEOPHYSICAL DATA

1. Introduction

Preliminary examination of the marine geophysical data indicates that the magnitude of the bottom loss measurements can be related to physiographic provinces and types of ocean bottom. As we shall show later, these measurements can be used to estimate some of the important parameters that describe the bottom of the ocean. The procedure that we suggest for the interpretation of reflection data combines our knowledge of the unconsolidated marine sediments and reflection of signals at a rough interface. It will be shown that roughness of the bottom frequently plays a dominant role in the areas where very little of the acoustical energy is reflected at the bottom of the ocean.

A physical approach is needed because a bottom loss measurement does not have general meaning or applicability in itself. The loss measurements must be considered in the context of the experiment and other geological and geophysical data. (Although we shall not pursue the matter, a loss measurement may be applicable only to equipment that works exactly in the same way as the measurements were made.) Our purpose in this is to supply some of the context and relationships that can give meaning to loss measurements. Perhaps it is needless to say it, but knowledge of the ocean, its bottom, and acoustical theory can be combined to predict sonar performance.

2. Summary

Much of the deep ocean is covered by sediments that can be described as sands and clays. Often the layers are a fraction of a meter thick and alternate. The range of the values of the average velocities and densities of the top few meters of sediments is such that the maximum range of reflection loss at normal incidence is approximately 7 to 14 dB. If the bottom is known to be sand or denser sediment, the losses would be expected to range from 7 to 10 dB. Inasmuch as low-frequency acoustic signals have longer wavelengths, these signals are reflected by the deeper more compacted layers and the reflection losses are smaller. The reflection from a layered smooth bottom is both frequency and angle dependent. A brief discussion is given in Appendix A. It would appear that bottom losses larger than 10 dB and certainly those larger than 14 dB must be due to some mechanism other than transmission into the bottom.

The results of the marine geophysical surveys indicate that the reflection losses are high in areas where the bottom is known to be rough and the losses are small in smooth areas. The physiographic charts such as those of Heezen and Tharp[1] are particularly useful in determining the location of the smooth and rough areas. To be useful for sonar performance prediction, the description of the bottom needs to be much more precise than smooth or rough. In the following, we give guide lines for quantitative interpretation of the marine geophysical reflection measurements.

a) Smooth and Slightly Rough Ocean Bottom

Over a smooth bottom at vertical incidence, 8 to 10 dB losses were measured at 3.5 kHz and slightly smaller dB losses were measured at 0.5 kHz. Even in the smoothest areas we frequently find that the vertical incidence bottom loss at 3.5 kHz is a little larger than that for 0.5 kHz. Also in smooth areas, the seismic profiles show smooth layered initial bottom and subbottom reflection as shown in Fig. 20. The precision echo soundings (12.5 kHz) usually show good bottom reflection and some sub-bottom reflections.
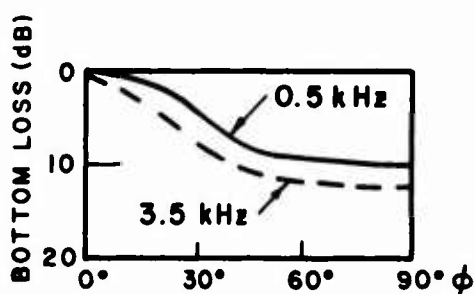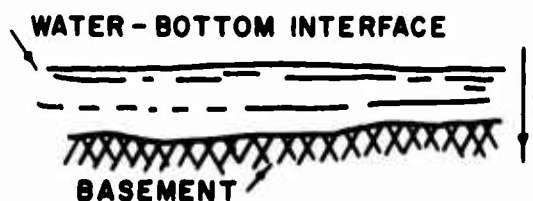
Fig. 20a. Smooth bottom, $\sigma < 0.1$ m (σ is the rms roughness).

Fig. 20b. Sketch of seismic profile.

As shown in Fig. 20a, the dependence of bottom loss on grazing angles is about that expected. In smooth areas, 0.5 and 3.5 Hz reflection coefficients of the ocean bottom tend to 0 dB at small grazing angles. This

-28-

is a typical result and is based upon the Marine Geophysical Survey data. The method used to estimate σ is discussed later and in Appendix B. As part of the routine geophysical surveys, bottom losses are measured with a 3.5 kHz echo sounder. These data show about 8 to 10 dB loss in smooth areas and appear to compare reasonably well with the acoustic reflectivity surveys. We mentioned earlier that the reflectivity correlates with the physiographic province. Measurements indicate that abyssal plains vary from very smooth, $\sigma < 0.1$ m , to slightly rough, $\sigma < 0.5$ m .

b) Intermediate Roughness of Bottom

Areas having an intermediate roughness have bottom losses that are frequency dependent. As shown in Fig. 21, the loss at 3.5 kHz is considerably higher than the loss at 0.5 kHz. The seismic profiles are essentially a graphic display of vertical incidence reflection data. The seismic signals are generally low-pass filtered to pass less than 0.2 kHz and as such are an indication of the 0.2 kHz reflection coefficient. In these areas, the seismic profiler data are good, i.e., the bottom and subbottom reflections are well defined, but the subbottom structure changes over short distances.

The amount of scattering depends upon the ratio of the roughness to the acoustic wavelength. In areas having $\sigma \simeq 1$ m , the 3.5 kHz signal has such a short wavelength that the sound is scattered at all grazing angles. Since the acoustic wavelength of 0.5 Hz is seven times larger, the same scale of roughness does not scatter the 0.5 Hz signals nearly as much. The 3.5 kHz vertical incidence losses range from 14 to 20 dB.

Some basins and many continental rises have intermediate roughness, $\sigma \simeq 1$ m .
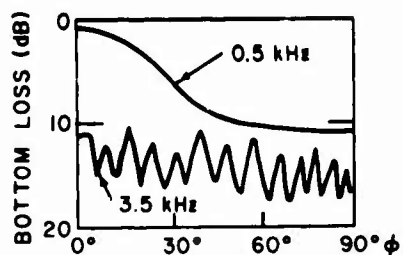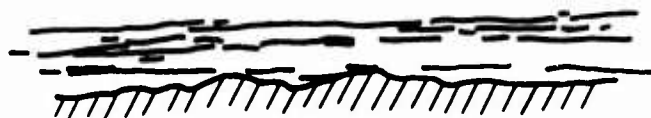
-29-

Fig. 21a. Intermediate roughness
$\sigma \simeq 1$ m.

Fig. 21b. Seismic profile.

c) Rough Areas

Rough areas appear to scatter the 0.5 and 3.5 kHz signals about the same amount, thus the bottom losses have the same range. Typical reflection losses are sketched in Fig. 22a. Several types of seismic profiles that are obtained in rougher areas are sketched in Fig. 22b. The shaded portion indicates the "basement" reflection. The scattering of sound in very rough areas such as ridges is primarily dependent upon the mean square slopes of the irregularities and independent of frequency. The fluctuations would be expected to be and are very large for small changes of geometry.
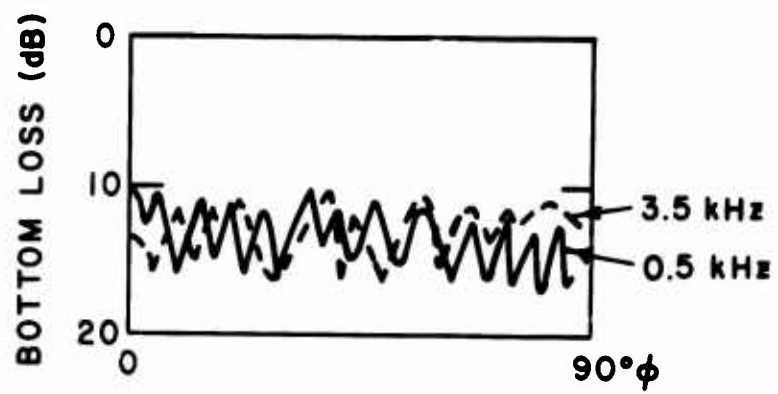
-30-
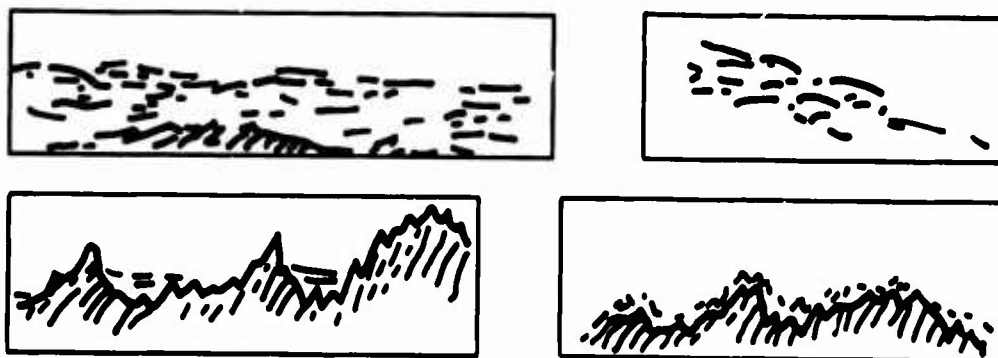
Fig. 22a.   Rough area, $\sigma > 2m$.

Fig. 22b.   Typical seismic profiles in rough areas.

3. Formulas and Discussion of Theory

The reflection and scattering theory is given in detail by Tolstoy and Clay (Ref. 4, Chapter 6). Results are summarized in the Appendices. In this section we give a few results and rules of thumb to estimate bottom roughness from bottom loss measurements. Some aspects of the measurement of roughness are discussed by Clay.[9]

a) Bottom Reflection - Smooth Area

As shown in Fig. 2, Part I, the reflected signal p_{ref} is, with the aid of the Eckart reflection coefficient[3] (Appendix Eqs.(B1)and(B2)) the following. (The reflection coefficient R_{12} or $\mathbb{R}$ is given by Eqs. (A1), (A5), , or (A11) in the Appendix. The choice of expression depends upon how complicated the bottom is.)

$$p_{ref}^2 = \frac{p_o^2 \langle \mathbb{R} \rangle^2}{(R_1 + R_2)^2} \tag{35}$$

where

$$\langle \mathbb{R} \rangle = \mathbb{R}\, e^{-2\gamma^2 \sigma^2} \tag{36}$$

p is acoustical pressure at unit distance

$$\gamma = \frac{2\pi}{\lambda} \sin \alpha \tag{37}$$

γ is the vertical component of wave number .

The exponential factor is e^{-1} for

$$\sigma = \frac{\lambda}{\pi\sqrt{2}\,\sin\phi} \tag{38}$$

-32-

and (38) can be used as a criterion of roughness. The bottom loss in dB can be written with the aid of Eq. (D1) and is

$$-20 \log_{10}\langle\mathbb{R}\rangle = -20 \log_{10}\mathbb{R} + 680 \frac{\sigma^2}{\lambda^2} \sin^2\phi \quad . \tag{39}$$

Equation (39) can be used to estimate the roughness of the area as follows: At signal grazing angles $\mathbb{R}$ tends to 1, thus the bottom loss is approximately the following:

$$[\text{Bottom loss for small } \phi] \simeq 680 \frac{\sigma^2}{\lambda^2} \sin^2\phi \quad . \tag{40}$$

The value of σ can be calculated with the aid of Eq. (40) for reflection coefficients that depend upon ϕ as sketched in Figs. 20 and 21.

For a given roughness, it is evident that the reflection loss, Eq. (37), is the same for a 100-Hz signal at 30° grazing angle and a 500-Hz signal at 6°. That is

at 100 Hz $\qquad \gamma = \frac{2\pi}{c} 100 \sin 30° = \frac{2\pi}{c} (0.5)(100)$

$$\tag{41}$$

at 500 Hz $\qquad \gamma = \frac{2\pi}{c} 500 \sin 6° = \frac{2\pi}{c} (0.1)(500) \quad .$

b) Bottom Scattering - Rough Area

In rough areas as shown in Fig. 22, most of the energy is scattered. Under these conditions, as shown by Eckart[3] and in Appendix C, the scattering is dependent upon the mean square slopes or σ and the correlation distance. The scattered sound is

-33-

$$p_{sc}^2 \simeq \mathbb{R}^2 \, SA \, \frac{P_o^2}{R_1^2 R_2^2} \tag{42}$$

A is the scattering area

S is the scattering function   .

Comparison of (35) and (42) shows that the reflected and scattered sounds have different functional dependence upon range.   The reflected signal depends upon range as $(R_1+R_2)^{-2}$, whereas the scattered signal p_{sc}^2 depends upon range as $R_1^{-2} R_2^{-2}$.   Calculation of the scattered sound requires knowledge of the scattering area   A .   Note that in many experimental measurements   A   has not been very well defined and only an apparent reflection coefficient has been determined.   The detailed discussion of a means of estimating   A   for particular experiments is given in Appendix C.

4. Conclusion

The marine geophysical data should be used with great care.   In smooth areas, the experimental data can be used to estimate the bottom parameters and the roughness.   Our ability to use surface reflection to make meaningful estimates of the sound velocity in the bottom layers decreases as the roughness increases.   In rough areas we must know the scattering area in order to estimate the scattering coefficient.

APPENDIX A

REFLECTION AT A SMOOTH BOTTOM

Much of the ocean bottom is covered by sediments that can be described as clays and sands and often these layers alternate. The acoustic velocity in the sediments shows an average increase with subbottom depth. The temperature gradient in the subbottom also causes an increase of acoustic velocity. Nafe and Drake[10] estimated the gradient to be from 0.4 sec^{-1} to 1.0 sec^{-1}. Depending upon the material, the acoustic velocity at the water sediment interface may vary from a few percent less than that in the water to somewhat higher. It is well known that the acoustic velocity in fluid-saturated unconsolidated sediments also depends upon the temperature. Because of the thermal gradient in the sediments, the acoustic velocity would also be expected to have an average increase as a function of depth. Laboratory acoustical measurements of recovered cores should be made at the proper temperatures. Data taken at some locations in the Pacific Ocean indicate that the acoustic velocity in the sediment near the water-sediment interface is less than the acoustic velocity in the water. Measurements of the acoustic velocity of the sediments in the Hatteras abyssal plain in the Atlantic Ocean have been around 1.6, 1.7 km/sec.[11] On the average, the acoustic velocity in the sediments increases with subbottom depth. The sound ray paths for both cases are shown in Fig. A1.

Experimental measurements of the attenuation of acoustic waves in sediments have shown that the materials absorb energy.[12] The absorption is dependent upon the kind of sediment and frequency. Generally the absorption is larger at higher frequencies. In addition to roughness, both the layering and absorption cause the reflection coefficient to be dependent upon frequency. In view of this, unqualified attempts to relate experimental data to a simple

non-layered model may be misleading. The conversion of compressional

wave energy to shear waves can also affect the reflection coefficient.
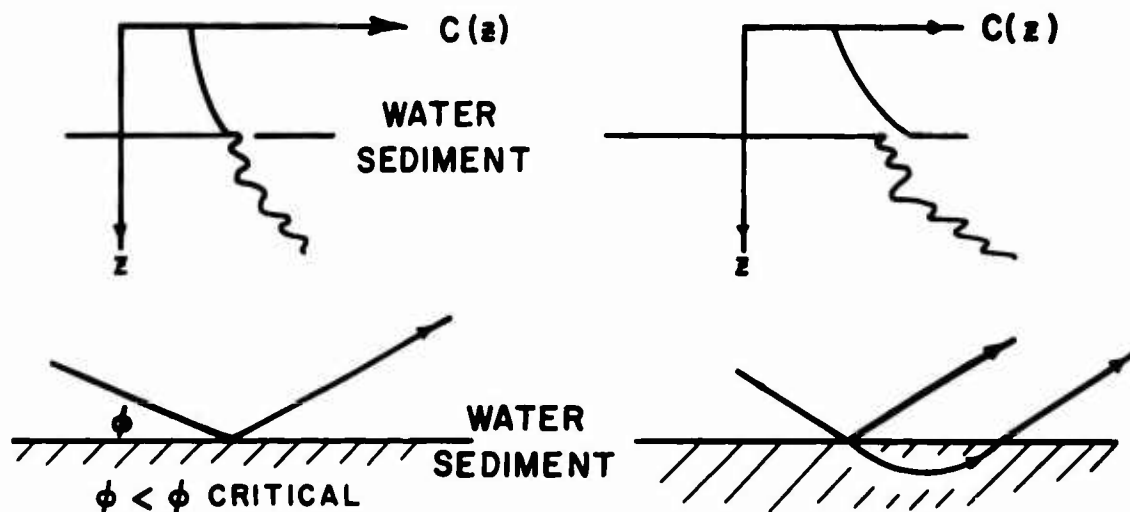

Fig. A1. Comparison of ray paths for higher and
lower velocities of sound at the water-sediment interface.

We assume that the reader is familiar with the reflection from the

plane interface between mediums 1 and 2 and the conditions for vertical

reflection. For the geometry shown in Fig. A2, the reflection coefficient

R_{12} as given by Tolstoy and Clay (Ref. 4, p. 30) is

$$R_{12} = \frac{\rho_2 \gamma_1 - \rho_1 \gamma_2}{\rho_2 \gamma_1 + \rho_1 \gamma_2} \tag{A1}$$

where

$$\gamma_1 = \frac{\omega}{c_1} \sin \phi_1 \qquad k_1 \sin \phi_1 \qquad , \qquad k = \frac{2\pi}{\lambda}$$

$$\gamma_2 = \frac{\omega}{c_2} \sin \phi_2 = k_2 \sin \phi_2 \qquad (A2)$$

and Snell's Law gives the relation between ϕ_1 and ϕ_2

$$\frac{\cos \phi_1}{c_1} = \frac{\cos \phi_2}{c_2} \qquad (A3)$$

ω = angular frequency

c_1 = velocity in medium 1

c_2 = velocity in medium 2

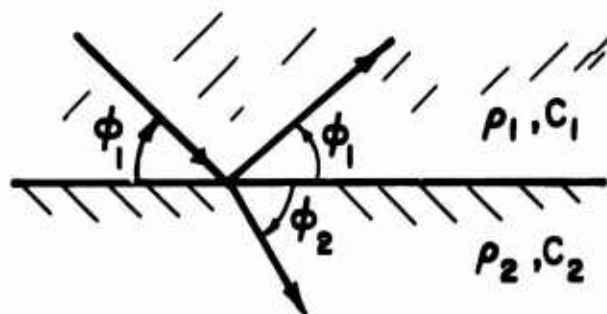ρ_1 and ρ_2 are the densities.

Fig. A2. Simple reflection.

Critical reflection occurs for grazing angles less than ϕ_{1c}

$$|R_{12}| = 1 \quad \text{for} \quad \phi_1 < \phi_{1c}$$

$$\cos \phi_{1c} = \frac{c_1}{c_2} \quad . \tag{A4}$$

The usual form of the reflection equation can be obtained by the substitution of (A2) into (A1) and the elimination of ω . The reflection from a layer is frequency dependent and, from Tolstoy and Clay (Ref. 4, p. 30), it is

$$\mathbb{R} = \frac{R_{12} + R_{23}\, e^{2i\gamma_2 h_2}}{1 + R_{12} R_{23}\, e^{2i\gamma_2 h_2}} \quad , \quad h_2 \text{ is layer thickness.} \tag{A5}$$

The reflection coefficient for a thin layer is shown in Fig. A3. The maxima and minima are caused by the interference of the reflections from the two interfaces. Although roughness is treated later, the dashed curve shows the effect of roughness on the coherent reflection coefficient. Multiple subbottom layers can be treated by the recursive technique given in Tolstoy and Clay.[4]
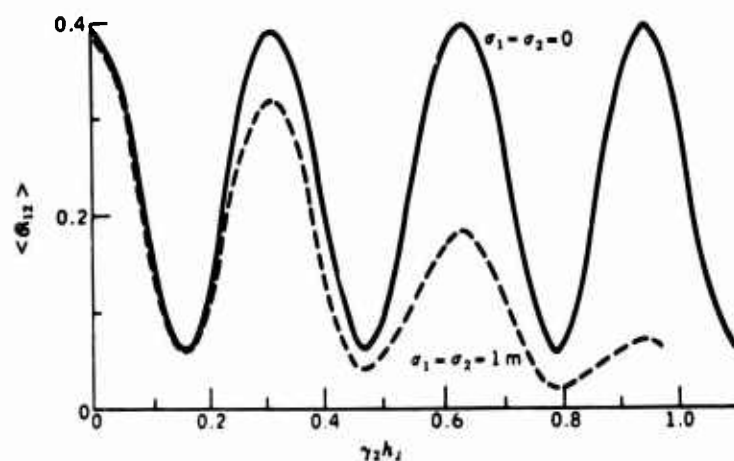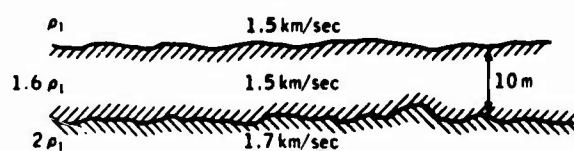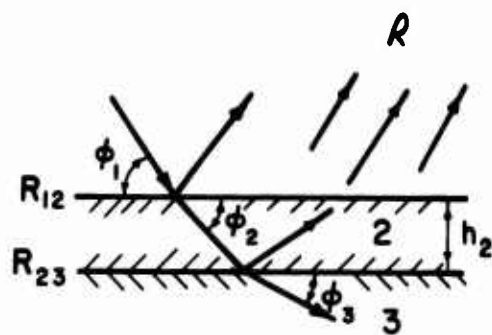
-38-

Fig. A3. Reflection from a layer. The solid curve is the reflection from a uniform layer $\sigma_1 = \sigma_2 = 0$. The dashed curve is the reflection from a slightly irregular layer $\sigma_1 = \sigma_2 = 1\ m$.

For grazing angles less than the critical angle at the 2-3 interface, R_{23} is complex and R_{23} can be written as follows

$$R_{23} = e^{i\chi}$$

$$a_2 < a_{2 \text{ crit.}} \qquad .$$

(A6)

The substitution of (A6) into (A5) and calculation of the absolute square of (A5) yields an extremely important result

$$|\mathbb{R}| = 1 \qquad . \tag{A7}$$

Thus the effective reflection coefficient of the layer is one, even though the top layer may have an acoustic velocity less than that in the water above the interface. In view of the observation that the sound velocity in sediments increases with depth of burial, one would generally expect to observe total reflection phenomena at shallow grazing angles.

Studies of reflection and transmission in deep sea sediments have shown that the absorption loss of acoustical energy in the sediments is considerably larger than the loss in water. As an example, we examine the characteristics of a layer having a small absorption. Following Tolstoy and Clay (Ref. 4, p. 221), we let

$$\gamma_2 = \gamma_2' + i \gamma_2'' \tag{A8}$$

where γ_2' is the vertical component of wave number in medium 2

γ_2'' is the absorption in medium 2.

(Here Snell's Law, Eq. (A3), is complex for complex angles.)

The substitution of (A8) in (A5) yields

$$\mathbb{R} = \frac{R_{12} + R_{23} e^{-2(\gamma_2'' h_2 - i\gamma_2' h_2)}}{1 + R_{12} R_{23} e^{-2(\gamma_2'' h_2 - i\gamma_2' h_2)}} \quad . \tag{A9}$$

The absorption coefficient γ_2'' is roughly proportional to frequency. At very high frequency, the signal reflected from the second interface is highly attenuated and $\mathbb{R}$ is approximately R_{12}. (The reflection from the first interface is also somewhat attenuated by the lossy bottom.)

$$\mathbb{R} \simeq R_{12} \tag{A10}$$

$$\text{for } \gamma_2'' h_2 \gg 1 \quad .$$

Equation (A9) tends to (A5) at low frequencies, and we would expect to observe the constructive and destructive interference of reflections from the two interfaces. A nice set of laboratory measurements has been made by Barnard et al.[13] Menotti et al.[14] have made field studies.

To conclude this section, we use Eq. (A1) to get an estimate of the gross range of the numerical values of R_{12} at vertical incidence.

-41-

At vertical incidence, $a_1 = a_2 = 90°$ and R_{12} is

$$R_{12}\bigg|_{vert} = \frac{\rho_2 c_2 - \rho_1 c_1}{\rho_2 c_2 + \rho_1 c_1} \quad \text{at vertical incidence.} \quad \text{(A11)}$$

Since the c_2 ranges from a few percent below c_1 to somewhat above in many marine sediments, the value of R_{12} mainly depends upon the densities. For a density range of 1.5 to 2.5, the reflection coefficient is in the following range

$$0.2 < R_{12} < 0.4 \quad \text{at vertical incidence} \quad \text{(A12)}$$

or the bottom loss ranges from 14 to 7 dB. In view of the average increase of ρc with increasing depth, one would expect to measure larger reflection coefficients at low frequencies.

APPENDIX B

REFLECTION AT A SLIGHTLY ROUGH BOTTOM

Irregularities of the interface cause scattering of the acoustic energy. Following the analysis of Eckart,[3] theoretical calculations are usually made for irregularity heights that are either small or very large compared to the acoustical wavelength (Ref. 4, pp. 193-220).

For small heights of irregularities, much of the signal is reflected in the specular direction and the reflection coefficient is referred to as the coherent reflection coefficient. On assuming that the irregularities have a Gaussian distribution and a root-mean-square roughness σ , the reflection coefficient for the reflection of signals from a simple rough interface is

$$\langle \mathbb{R} \rangle = R_{12} e^{-2\gamma^2 \sigma^2}$$

or

$$\langle \mathbb{R} \rangle = R_{12} e^{-2k^2 \sigma^2 \sin^2 \phi} \tag{B1}$$

$$k = \omega/c \qquad .$$

The magnitude of the acoustical pressure squared (ignoring the time dependence) is given by the image method and is

$$p_{ref}^2 = \frac{p_o^2}{(R_1 + R_2)^2} \langle \mathbb{R} \rangle^2 \tag{B2}$$

where the geometry is shown in Fig. B1 and p is the pressure at unit distance. Experimental data are shown and compared to theory in Fig. (B2).

-43-

where
$$\langle pp^* \rangle \;=\; p_{ref}^2 + p_{sc}^2$$

$$\langle p_o p_o^* \rangle \;=\; p_o^2 \qquad \text{for} \qquad \langle R^* \rangle^2 = 1$$

$$\langle p \rangle^2 \;=\; p_{ref}^2 \qquad .$$

p_{sc}^2 is the sound scattered by the irregularities on the surface. This energy is incoherent and while its intensity is larger in the specular direction, the sound beam is considerably broadened. The scattered sound is usually referred to as reverberation.
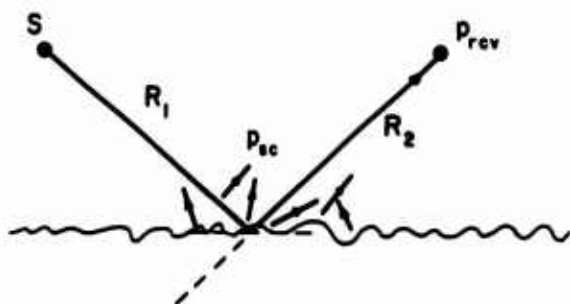

Fig. B1. Reflection and scattering.

A comparison of Eq. (B1) and experiment is the dashed line in Fig. B2. The dashed line is proportional to $\langle R \rangle^2$ and the solid line is proportional to the sum of the coherent reflected signal and the incoherent scattered energy. Notice that the scattered contribution is about 0.1 at high frequency or large $\gamma \sigma$.
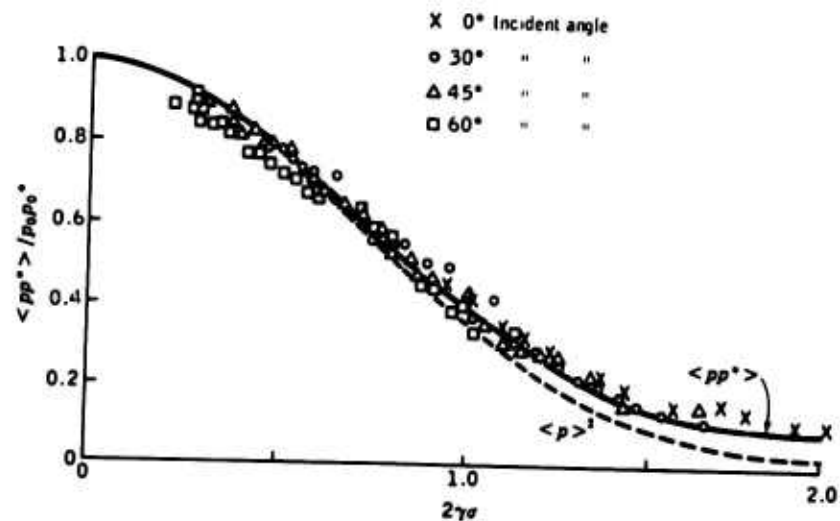
Fig. B2. Mean radiation scattered by a rough surface.
The radiation scattered in the specular direction for
0°, 30°, 45°, and 60° was measured by Proud, Beyer,
and Tamarkin.[8] Their data for the different directions
have been combined in one figure, and the original
notation is changed.

APPENDIX C

REFLECTION AT A VERY ROUGH BOTTOM

At large roughness compared to the acoustical wavelengths, the geometrical dependence of the scattered radiation is different from the specular case. As shown in Fig. 3, Part I, the area A is assumed to be illuminated and the energy is incoherently scattered by each part of the surface. The scattered sound p_{sc}^2 is

$$p_{sc}^2 = \frac{S A p_o^2}{R_1^2 R_2^2} \tag{C1}$$

where S is the scattering coefficient. For high frequencies and a very rough surface Eckart found that S is dependent upon the mean square slope of the surface $\langle \zeta'^2 \rangle$ and independent of frequency. Comparison of (B2) and (C1) shows that the reflected and scattered sound have different functional dependence upon range (Ref. 4, p. 213). Different choices of boundary conditions and correlation functions of the irregular surface lead to different values of S.[6] The effect of different correlation functions is discussed in some detail in Part I. Following Eckart, Tolstoy and Clay used a boundary condition that assumes the differential area to be a plane surface and a Gaussian correlation function. They found S to be the following:

$$S \simeq \frac{\mathbb{R}_{12}^2}{8\pi\langle \zeta'^2 \rangle} \tag{C2}$$

where $\langle \zeta'^2 \rangle$ is mean square slope.

Recently Horton et al.[6] measured the scattered sound for this case and compared the experimental results with their theoretical calculations. The correlation function of their surface is approximately our ψ_ℓ , shown in Fig. 10, Part I. A figure from their paper is our Fig. C2. For these experiments, $\left| \mathbb{R}_{12} \right| = 1$ and a directional source was used to illuminate a known scattering area. The equation of the scattering function is our Eq. (23a), Part I.

On the average, scattered waves add randomly. However, for a particular source, receiver, and rough surface, repeated transmissions are reproducible. Translation of the rough surface causes the scattered waves to add differently. A small change of the source or receiver position also causes the waves to add differently. Thus one would expect the scattered signal level to have large fluctuations and the 20 dB fluctuations found by Horton et al. would be expected. The curves shown in Fig. C1 are the average of five runs. The fluctuations are present but reduced.

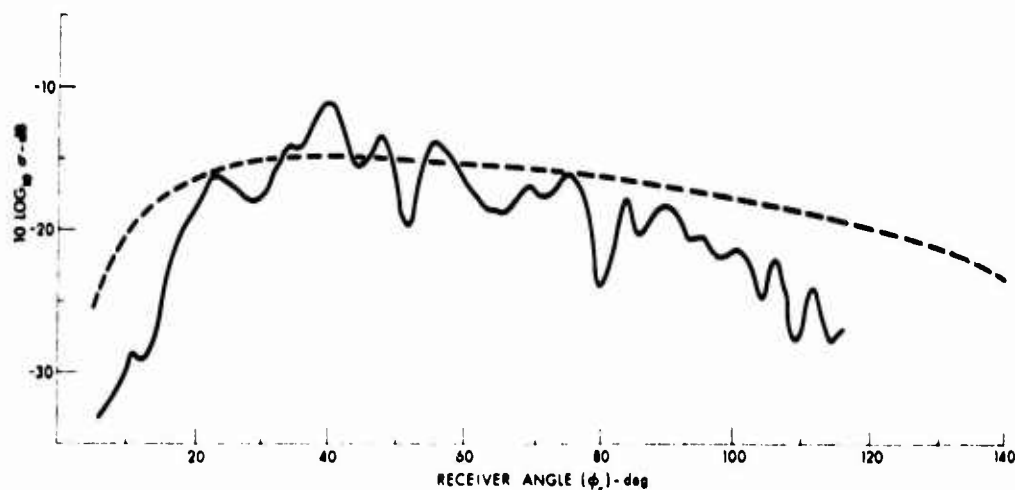Fig. C1. The scattering coefficient for $\phi_i = 40°$ and $f = 100$ kHz. This is an average of five measurements at different positions on the model surface. The solid curve is experimental and the dashed curve is from Eq. 8 (in Horton et al.[6]).

The data in Fig. C1 show another important feature of the scattered field. The scattered radiation is rather diffuse and slightly peaked in the specular direction. The scattering coefficient is about -20 dB. This type of scattering coefficient is used in Eq. (C1).

If the bottom is illuminated by means of an omnidirectional source such as a shot and the scattered radiation is received by hydrophone, it may be difficult to determine what the illuminated area is. Furthermore, sound reflected or scattered by subbottom layers may be present. We believe that much care must be used in the interpretation of data taken in rough areas. The problem is somewhat ill defined. In addition to scattering loss numbers, the readers of reports should be given samples of the echo soundings, seismic profiles, and graphic records of the reflection signals for each reflection study. Presumably the signals and sources of the quoted loss numbers would be identified on the records.

Let us return to equation (C1) and use it to estimate the scattered sound for a typical experiment. We assume that the source is a shot and the receiver filters, squares, and averages p^2 for Δt sec. The effective illumination area is essentially given by the first Δt sec after the initial scattered signal arrives ($\Delta t \gg$ the source signal duration).

The geometry is shown in Fig. C2. (The water is assumed to be iso-velocity.)

Fig. C2. Scattering area.
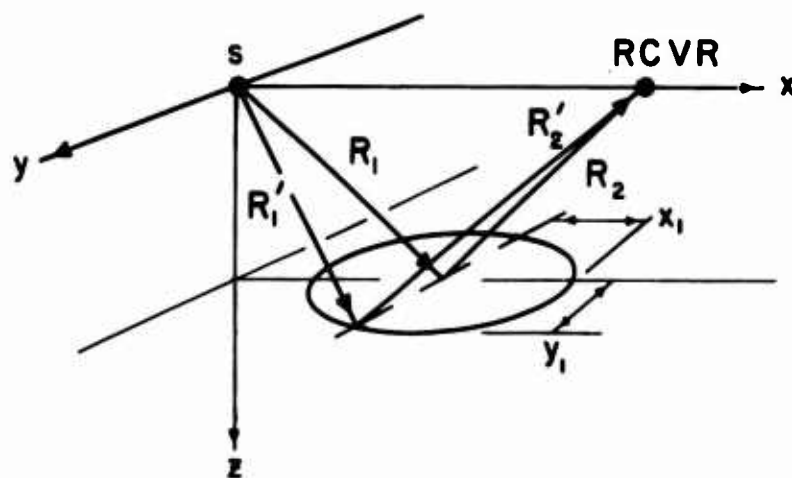
To determine A , we first estimate x_1 and y_1 in Fig. C2.
The travel times in the specular direction, $R_1 = R_2$, are

$$t_1 + t_2 = 2R_1/c_1$$

$$t_1' + t_2' = 2R_1'/c \qquad\qquad (C3)$$

$$\Delta t = (t_1' + t_2') - (t_1 + t_2)$$

by the Sagitta formula

$$y_1 \simeq \sqrt{2(\Delta t c)R_1} \qquad\qquad . \qquad (C4)$$

For the grazing angle

$$x_1 \simeq y_1/\sin \alpha$$

$$\simeq y_1 R_1/h \qquad . \qquad (C5)$$

The area of an ellipse is

$$A = \pi x_1 y_1 = 2\pi \frac{\Delta t c}{h} R_1^2 \qquad . \qquad (C6)$$

The scattered sound, in specular direction and averaged over Δt , is as follows:

$$\overline{p_{sc}^2}\bigg|_{\Delta t} = p^2(l) \, \mathbb{R}^2 \, S \, \frac{A}{R_1^4}$$

$$\simeq p_1^2(l) \, \mathbb{R}^2 \, \frac{S}{R_1^2} \, \frac{2\pi \Delta t c}{h} \qquad . \qquad (C7)$$

For constant Δt and water depth, h , $\overline{p_{sc}^2}\bigg|_{\Delta t}$ has a dependence of R_1^{-2} . This is superficially similar to the ordinary reflection equation.

Many times, reflection coefficients are computed on the basis of the specular reflection equation. Although it is incorrect, we proceed and assume an apparent reflection coefficient $\mathbb{R}_{ap}$. With the aid of Eq. (B2) the corresponding scattered sound in the specular direction is

$$p_{sc}^2 = p_o^2 \, \frac{\mathbb{R}_{ap}^2}{4 R_1^2} \qquad . \qquad (C8)$$

The following value of $\mathbb{R}^2_{ap}$ is obtained by equating (C7) and (C8):

$$\mathbb{R}^2_{ap} = \mathbb{R}^2 S \left(\frac{8\pi\Delta tc}{h}\right) \quad . \qquad (C9)$$

In the deep ocean h is about 20,000 ft. On assuming $\Delta t \simeq 0.01$ sec, the third factor in Eq. (C9) is

$$8\pi\Delta t/h \simeq 2\pi \times 10^{-2}$$

and the apparent reflection coefficient is

$$\mathbb{R}^2_{ap} \simeq 2\pi \mathbb{R}^2 S \times 10^{-2} \quad . \qquad (C10)$$

As an example for scattering in a very rough area, let us assume that the rms slope of all of the nooks, crannies, and rocks is 15°,

$$\langle \zeta'^2 \rangle \simeq \tan^2 15° \quad .$$

Substitution of the value into Eq. (C2) yields

$$S \simeq 10^2/(56\pi) \quad . \qquad (C11)$$

The apparent reflection coefficient is

$$\mathbb{R}^2_{ap} \simeq \frac{1}{27} \mathbb{R}^2 \qquad (C12)$$

and conversion to dB yields

$$10 \log \mathbb{R}_{ap} \simeq -14 \text{ dB} + 20 \log \mathbb{R} \qquad . \qquad \text{(C 13)}$$

Near vertical incidence $20 \log \mathbb{R}$ is of the order of -10 dB and decreases to zero at grazing incidence. Thus we would expect the following

$$
\begin{aligned}
10 \log \mathbb{R}_{ap} &\simeq -24 \text{ dB} && \text{vertical} \\
&\simeq -14 \text{ dB} && \text{grazing}
\end{aligned}
$$

in a rough area.

APPENDIX D

SUMMARY

The dependence of the scattered sound upon frequency and the incident and reflected angles is very useful in deciding whether the roughness is greater or less than the acoustical wavelength. The basic dependence of the reflection coefficient and S upon ϕ is sketched in Fig. D1. Large fluctuations are expected. As an alternative let us consider the scattered and reflected sound as a function of roughness. Figure D2 illustrates its dependence upon the root-mean-square roughness σ , acoustical wavelength, and incident angle.
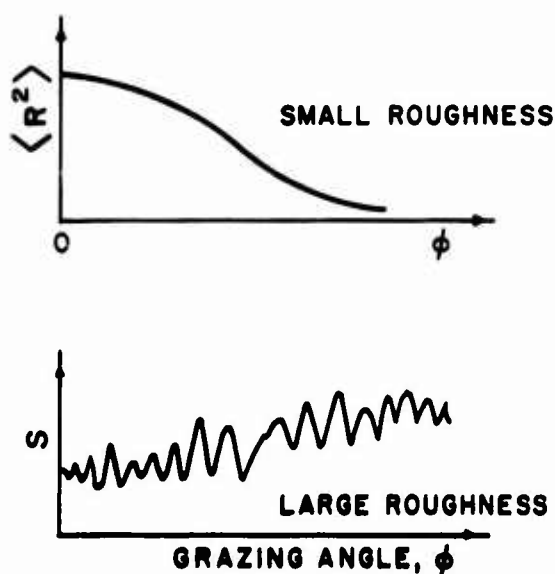

Fig. D1. Comparison of large and small roughness as a function of ϕ .

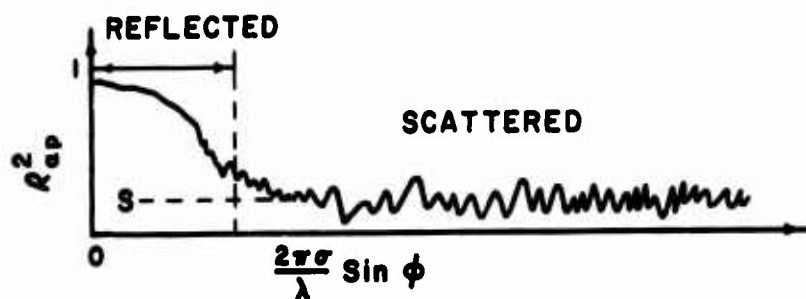Fig. D1. Comparison of large and small roughness as a function of ϕ .

Fig. D2. For $\mathbb{R} = 1$, apparent reflection coefficient $\mathbb{R}_{ap}$.

The conversion to apparent bottom reflection is shown in Fig. D3.
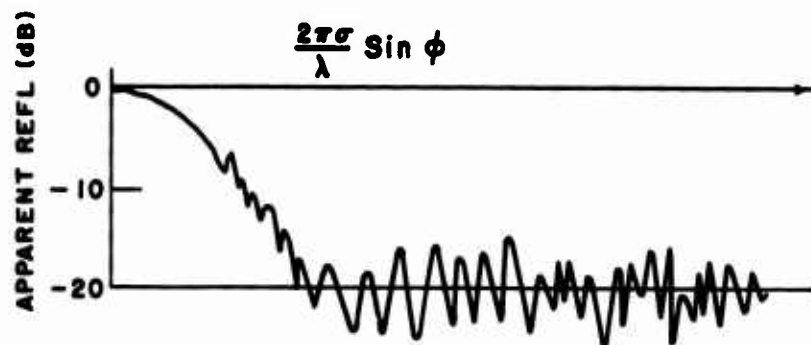We assumed that the scattered coefficient is approximately -20 dB.

Fig. D3. Apparent bottom reflection.

Often data are expressed as bottom reflection loss, in dB as a function of frequency and angle. Equation (B1) expressed in dB is as follows:

$$-10 \log_{10} \langle R \rangle = -[20 \log_{10} \mathbb{R}] + 20[2\gamma^2 \sigma^2] \log_{10} e$$

$$\simeq -20 \log_{10} \mathbb{R} + 680 \frac{\sigma^2}{\lambda^2} \sin^2 \phi \qquad (D1)$$

where $\quad \gamma = \frac{2\pi}{\lambda} \sin \phi$.

ACKNOWLEDGMENT

REFERENCES

1. B. C. Heezen and M. Tharp, "Physiographic diagram, Atlantic Ocean (Sheet 1)," Geol. Soc. Am. Special Paper 65 (1957).

2. L. M. Brekhovskikh, *Waves in Layered Media* (Academic Press, New York, 1960), 561 pp.

3. C. Eckart, "The scattering of sound from the sea surface," J. Acoust. Soc. Am. $\underline{25}$, 566-570 (1953).

4. I. Tolstoy and C. S. Clay, *Ocean Acoustics* (McGraw-Hill Book Co., New York, 1966), 293 pp.

5. C. W. Horton, Sr., and T. G. Muir, "Theoretical studies on the scattering of acoustic waves from a rough surface," J. Acoust. Soc. Am. $\underline{41}$, 627-634 (1967).

6. C. W. Horton, Sr., S. K. Mitchell, and G. R. Barnard, "Model studies on the scattering of acoustic waves from a rough surface," J. Acoust. Soc. Am. $\underline{41}$, 635-643 (1967).

7. C. S. Clay, J. Ess, and I. Weisman, "Lateral echo soundings of the ocean bottom on the continental rise," J. Geophys. Res. $\underline{69}$, 3823-3835 (1964).

8. J. M. Proud, Jr., R. T. Beyer, and P. Tamarkin, "Reflection of sound from randomly rough surfaces," J. Appl. Phys. $\underline{31}$, 543-552 (1960).

9. C. S. Clay, "Coherent reflection of sound from the ocean bottom," J. Geophys. Res. $\underline{71}$, 2037-2046 (1966).

10. J. E. Nafe and C. L. Drake, "Physical properties of marine sediments," in The Sea, Vol. 3, ed. M. N. Hill (Interscience Publishers, New York, 1961), pp. 794-815.

11. C. S. Clay and P. A. Rona, "Studies of seismic reflections from thin layers on the ocean bottom in the Western North Atlantic," J. Geophys. Res. 70, 855-869 (1965).

12. A. B. Wood and D. E. Weston, "The propagation of sound in mud," Acustica 14, 156-162 (1964).

13. G. R. Barnard, J. L. Bardin and W. B. Hempkins, "Underwater sound reflection from layered media," J. Acoust. Soc. Am. 36, 2119-2123 (1964).

14. F. R. Menotti, S. R. Santaniello, and W. R. Schumacher, "Studies of observed and predicted values of bottom reflectivity as a function of incident angle," J. Acoust. Soc. Am. 38, 707-714 (1965).

DOCUMENT CONTROL DATA · R & D

(Security classification of title, body of abstract and indexing annotation must be entered when the overall report is classified)

1. ORIGINATING ACTIVITY *(Corporate author)*	2a. REPORT SECURITY CLASSIFICATION
Hudson Laboratories of Columbia University Dobbs Ferry, New York 10522	Unclassified 2b. GROUP

3. REPORT TITLE

ESTIMATION OF THE STATISTICAL PROPERTIES OF THE OCEAN BOTTOM
Part I: A Survey of Theory and Experiment
Part II: Interpretation of Marine Geophysical Data

4. DESCRIPTIVE NOTES *(Type of report and inclusive dates)*

Technical Report

5. AUTHOR(S) *(First name, middle initial, last name)*

C. S. Clay

6. REPORT DATE	7a. TOTAL NO. OF PAGES	7b. NO. OF REFS
December 1967	67	14

8a. CONTRACT OR GRANT NO. Nonr-266(84) b. PROJECT NO. c. d.	9a. ORIGINATOR'S REPORT NUMBER(S) Technical Report No. 138 9b. OTHER REPORT NO(S) *(Any other numbers that may be assigned this report)*

10. DISTRIBUTION STATEMENT

Document cleared for public release and sale; its distribution is unlimited.

11. SUPPLEMENTARY NOTES	12. SPONSORING MILITARY ACTIVITY Office of Naval Research, Code 466.

13. ABSTRACT

The reflection and scattering of acoustic signals by the bottom of the ocean depends upon the physical properties of the bottom and the wavelength spectrum of the signals. On the basis of the frequency and grazing angle dependence of the reflected or scattered signals, physical properties such as the densities, acoustic velocities of subbottom layers, and the rms roughness of the layers can be estimated.

14. KEY WORDS	LINK A		LINK B		LINK C	
	ROLE	WT	ROLE	WT	ROLE	WT
Estimation statistical						
Ocean bottom						
Marine geophysical						